Polyolefin thermoplastic elastomers from 1-octene chain-walking polymerization

Giuseppe Leone [a,*], Massimiliano Mauri [a], Ivana Pierro [a,b], Giovanni Ricci [a],

Maurizio Canetti [a], Fabio Bertini [a,*]

[a] *Istituto per lo Studio delle Macromolecole C.N.R., Via Bassini 15, I-20133 Milano, Italy*

[b] *Dipartimento di Scienze Chimiche, Università di Napoli Federico II, Complesso Monte S. Angelo,via Cintia, I-80126 Napoli, Italy*

* Corresponding author.

E-mail addresses: leone@ismac.cnr.it (G.Leone), bertini@ismac.cnr.it (F.Bertini)

ABSTRACT

This work reports the polymerization of 1-octene to yield semicrystalline, branched poly(ethylene)–like materials with high molecular weight and narrow molecular weight distribution. The polymerization of 1-octene was catalyzed by an α-diimine Ni(II) complex [(ArN)C(CH_3)–(CH_3)C(NAr)]$NiBr_2$ [Ar = 2,6-(*i*Pr)$_2C_6H_3$], in combination with different aluminum alkyls, *i.e.*, Et_2AlCl, MAO and MMAO. The effect of the aluminum alkyl, monomer concentration, polymerization temperature and Al/Ni ratio on the activity, selectivity of monomer insertion, polymers microstructure, and structure/properties is investigated. The results indicate the possibility to tune the polymer microstructure, which in turn strongly affects the structure, thermal and mechanical polymer properties. Mechanical testing carried out by uniaxial stretching until failure and step-cycle tensile experiments served to establish these materials as a new class of polyolefin thermoplastic elastomers with different performances depending on the microstructure and crystallinity.

Keywords:

Thermoplastic elastomers; Polyolefins; 1-octene polymerization; Nickel; Mechanical properties

1. Introduction

Poly(olefin)s have become the world's most common synthetic polymers, with current annual capacity of about 180 million tons [1]. The current trend suggests that POs global installed capacity growth is expected to increase by 4–5 % over the next few years. This growth will be powered by a series of breakthroughs in development of different classes of well-defined transition metal complexes [2-4], living insertion/coordination polymerization [5], and synthesis of differentiated and more complex polymers and crystalline structures [6,7]. Ethylene and α-olefin thermoplastic elastomers are the most versatile poly(olefin)s in today's market. They are used in different applications ranging from packaging to lightweight engineering plastics for automotive, textiles, rubbers, electrical and thermal insulation, and earthquake-proof pipes for safe transport of water and gas.

Thermoplastic elastomers (TPEs) are a class of (co)polymers that combine the processing advantages (*i.e.*, they can be processed by injection molding, extrusion and blow molding) and recycling potential of thermoplastics with the flexibility, low modulus, and soft touch of elastomers. TPEs can be repeatedly stretched without permanent deformation and, unlike rubber-like elastomers, they do not require curing or vulcanization. With respect to other TPE types, polyolefin TPEs have received considerable attention because of their better chemical resistance, lower density and excellent weatherability. In addition, low cost and wide availability of sustainable commodity ethylene, propylene and α-olefin monomers makes polyolefin TPEs more desirable.

Ethylene copolymers with α-olefins (*i.e.*, 1-hexene, 1-octene) are one of the most used TPEs with high performances with respect to the elastomeric properties of low modulus and high recovery from large deformation. A key aspect in the development of such high performance TPEs is the comonomer distribution, the degree of crystallinity and the distribution of crystalline domains. Furthermore, better performances have been achieved with block copolymers rather than with random ones. In random copolymers the statistical distribution of crystallizable chain lengths results in a broad crystal size, while in block copolymers the crystalline structure is better organized, and the rubbery block is more easily stretched to higher strain [8,9]. Random olefin copolymers from copolymerization of ethylene with 1-octene exhibit narrow molecular weight distribution, homogenous composition and good mechanical properties and are commercialized as TPEs by DOW and ExxonMobil [10].

Recently, different classes of transition metal complexes and new polymerization strategies have been developed to fabricate polyolefin TPEs. Coates and Waymouth reported the synthesis of stereoblock poly(propylene)s (PPs), having isotactic and atactic blocks, with "oscillating"

zirconocene catalyst [11]. In 2006, new elastomeric multiblock poly(olefin)s were obtained through a chain shuttling polymerization, and commercialized by DOW [12]. Another elegant technique to produce high performance TPEs is the fabrication of well-defined graft polymers featuring amorphous backbones and crystalline side-chains by ExxonMobil [13,14]. This strategy was applied by Coates and Fredrickson to the synthesis of graft copolymers containing semicrystalline PP side-chains and amourphous ethylene/propylene or ethylene/1-octene copolymer backbones [15]. Numerous efforts have been also made to develop cost-effective post-metallocene based catalysts, and living olefin polymerizations. For example, a living bis(phenoxyimine)Ti(IV) complex has been used to fabricate syndiotactic PP-*block*-poly(E-*co*-P)-*block*-syndiotactic PP [16], and a living dimethyl, cyclopentadienyl, amidinate hafnium complex has been reported to give amourphous 1,6-heptadiene/propene/1,6-heptadiene block copolymers [17].

Another great innovation was the discovery of late transition metal complexes bearing α-diimine ligands [18-22]. The application of Ni(II) and Pd(II) complexes allowed the synthesis of branched, hyperbranched [23-25], and block (co)polymers [26,27] with high activity, stereoselectivity and in a living fashion. Dramatic differences in microstructure, physical and mechanical properties of poly(olefin)s obtained from late metal complexes were observed with respect to the traditional Ziegler-Natta and metallocene technology [28-34]. For example, a living C2-symmetric Ni(II) diimine chiral complex has been reported to form regio-block PPs featuring three or five blocks, with exceptional elastic properties in terms of true stress at break and elastic recovery [35]. Also our group exploited the synthesis of multiblock (co)polymers catalyzed by α-diimine Ni(II) based catalysts and, very recently, we succesfully reported the fabrication of di- and three-block copolymer from sequential monomer addition of 1-dodecene and ethylene [36]. Each block exhibited distinct features from semicrystalline to amorphous, taking advantage of the different mechanism involved in the polymerization of 1-dodecene (chain-straightening) and ethylene (chain-walking).

This work extends our previous studies on the polymerization of higher linear α-olefins, focusing on the polymerization of 1-octene. The effect of monomer concentration, reaction temperature, Al/Ni mole ratio and aluminum alkyl type (*i.e.*, Et_2AlCl, MAO and MMAO) on productivity, selectivity of monomer insertion and polymer structure/properties (*i.e.*, total branching, branch-type, crystallinity and thermal behavior) is discussed. The mechanical behavior of the obtained polymers was investigated by uniaxial stretching until failure and step-cycle tensile tests. To the best of our knowledge, this is the first example of 1-octene polymerization which leads to semicrystalline poly(ethylene-*co*-propylene-*co*-1-octene)-like materials with excellent elastomeric behavior.

2. Experimental

2.1. Materials

Manipulations of air- and/or moisture-sensitive materials were carried out under an inert atmosphere using a dual vacuum/nitrogen line and standard Schlenk-line techniques. Toluene (Fluka, > 99.5% pure) was refluxed over Na for about 8 hours and then distilled and stored over molecular sieves under nitrogen. Diethylaluminium chloride (Et_2AlCl, Fluka), methylaluminoxane (MAO) (10 wt. % solution in toluene, Aldrich), and modified- methylaluminoxane (MMAO, 7 wt. % solution in heptane, Akzo Nobel) were used as received. The α-diimine Ni(II) complex [2,6-(*i*Pr)$_2$C$_6$H$_3$N=C(CH$_3$)−(CH$_3$)C=N2,6-(*i*Pr)$_2$C$_6$H$_3$)]NiBr$_2$ (Ni-1, Scheme 1) was synthesized according to the literature [37]. 1-Octene (Aldrich, 98% pure) was refluxed over CaH_2 for about 4 hours, then distilled via trap-to trap and, finally, stored under dry nitrogen and kept at –30°C. Deuterated solvent for NMR measurements ($C_2D_2Cl_4$) (Cambridge Isotope Laboratories, Inc.) was used as received.

2.2 Polymerization

Polymerizations were carried out in a 25 mL round-bottomed Schlenk flask. The reactor was first dried by heating at 110 °C and then vacuum was applied for 1 hour. Toluene, 1-octene, Et_2AlCl and a toluene solution of Ni-1 (2 mg/mL) were transferred into the reactor vessel in that order. Polymerization was quenched with methanol containing a small amount of hydrochloric acid. The precipitated polymers were collected by filtration, repeatedly washed with fresh methanol and then dried to constant weight.

2.3 Characterization

For ^{13}C NMR, about 100 mg of copolymer was dissolved in $C_2D_2Cl_4$ in a 10 mm tube. HDMS (hexamethyldisiloxane) was used as internal chemical shift reference. The spectra were recorded on a Bruker NMR AVANCE 400 Spectrometer operating at 100.58 MHz (^{13}C) in the PFT mode working at 103 °C. The applied conditions were the following: 10 mm probe, 90° pulse angle; 64 K data points; acquisition time 5.56 s; relaxation delay 20 s; 3−4K transient. Proton broad-band decoupling was achieved with a 1D sequence using bi_waltz_16_32 power-gated decoupling. ^{1}H NMR spectroscopy was used to determine overall branching [38]. The fraction of 8,1-insertions was calculated from the equation reported by Brookhart [39]. ^{13}C NMR spectroscopy was used to

examine the types of branches. The quantitative analysis was based on the equations reported by Galland [40].

The molecular weight average (M_n), the molecular weight distribution (M_w/M_n), and the intrinsic viscosity ($[\eta]_w$) were obtained by a high temperature Waters GPCV2000 size exclusion chromatography (SEC) system using two online detectors: a differential viscometer and a refractometer. The experimental conditions consisted of three PL Gel Olexis columns, *o*-DCB as the mobile phase, 0.8 mL/min flow rate, and 145°C temperature. The calibration of the SEC system was constructed using eighteen narrow M_w/M_n polystyrene standards with molar weights ranging from 162 to 5.6×10^6 g/mol. For SEC analysis, about 12 mg of polymer was dissolved in 5 mL of *o*-DCB with 0.05% of BHT as antioxidant.

Differential scanning calorimetry (DSC) measurements were performed on a Perkin–Elmer Pyris 1 instrument equipped with a liquid nitrogen device. The scans were carried out from -120 to 200 °C under helium atmosphere using heating and cooling rates of 20 °C/min.

Wide Angle X-ray Diffraction (WAXD) data were obtained at 18 °C using a Siemens D-500 diffractometer equipped with a Siemens FK 60-10 2000W tube (Cu K_α radiation, λ = 0.154 nm). The operating voltage and current were 40 kV and 40 mA, respectively. The data were collected from 5 to 35 2θ° 0.02 2θ° intervals.

SAXS measurements were conducted at 18 °C with a Kratky Compact Camera. Monochromatized Cu K_α radiation (λ = 0.154 nm) was supplied by a stabilized Siemens Krystalloflex 710 generator and a Siemens FK 60-10 2200 W Cu target tube operated at 40 kV and 45 mA. The scattered intensity was counted in different ranges of 2θ°, by using a step scanning proportional counter with pulse height discrimination, the data were successively corrected for blank scattering and desmeared. The internal surface of the polymers was calculated as proposed by the Porod approach for non-particulate system [41].

The materials for the mechanical characterization were molded in a heated press at 90 °C and 50 bar for 5 min, then the press plates were cooled at 20 °C/min to room temperature. Films with a thickness of about 150 μm were produced. Tensile dog-bone-shaped specimens (length overall 75 mm, gauge length 25 mm, and width of narrow section 4 mm) were analyzed at 20 °C using a Zwick Roell ProLine Z010 mechanical tester equipped with a XforceP (50 N) load cell at a constant crosshead rate of 15 mm/min. In the hysteresis experiments performed at various strains, the specimens were cyclically loaded and unloaded in uniaxial tension.

3. Results and Discussion

3.1. Polymerization of 1-octene

In our recent work, we screened Et_2AlCl in combination with Ni-1 complex for the polymerization of 1-hexene, 1-octene and 1-dodecene at different monomer concentration [36]. Polymerization gave branched, semicrystalline poly(ethylene)-like materials with narrow molecular weight distribution. Herein, we report extension of our studies about the Ni(II)–catalyzed 1-octene polymerization by expanding the range of monomer feedstock concentration from 0.2 to 3.0 mol/L. Additional polymerizations were carried out modifying the Al/Ni mole ratio, the polymerization temperature and using Ni-1 in combination with different alumoxanes (*i.e.*, MAO and MMAO). Polymerization results are summarized in Table 1.

Catalyst Ni-1/Et_2AlCl displayed good activity for 1-octene polymerization, with products obtained in the order of grams. Although turnover frequency (TOF) was strongly affected by mass transfer limitations, the calculated TOFs increased with monomer concentration. There is no substantial change in monomer conversion with the increase of 1-octene feedstock concentration. This behaviour can be accounted to the higher exothermic character at the beginning of the reaction and to the increased viscosity of the reaction mixture.

The effect of Al/Ni ratio was investigated for Ni-1/Et_2AlCl at monomer concentration of 1.0 mol/L. The activity did not increase with Al/Ni ratio from 10 to 500, meaning that formation of the active species is apparently complete (but not necessarily quantitative) and sufficient for Al/Ni = 10. The molecular weight distribution of the obtained polymers was monomodal and ranged from 1.37 (Table 1 entry 10, Al/Ni = 10) to 1.89 (Table 1 entry 12, Al/Ni = 500), indicating a single site catalytic system.

The particular aluminium alkyl plays an important role for polymerization activity, molecular weight and molecular weight distribution. Ni-1/MAO and Ni-1/MMAO were generally less active than Ni-1/Et_2AlCl. This result could be likely due to the fact that cationic nickel-alkyl species, formed by Ni-1 and Et_2AlCl, may stay in equilibrium between chloro-bridged and cationic alkyl species due to the less steric bulk and stronger nucleophilic nature of Et_2AlCl [42,43]. Such a close interaction would stabilize the catalytically active species, leading to a higher monomer conversion. In addition, the polymers from Ni-1/MAO and Ni-1/MMAO had higher molecular weight and larger molecular weight distribution.

The effect of polymerization temperature was investigated in the case of Ni-1/Et_2AlCl. By increasing the temperature from 0 to 22 °C yielded a threefold 1-octene conversion increase, while a further temperature rise to 50 °C had no significant influence on the activity (Table 1, entry 5, 13, 14). Increasing the reaction temperature, the obtained polymers had higher molecular weight,

meaning that chain transfer and termination reactions are reduced as compared to the chain propagation at elevated temperature [38,39,44].

3.2 Structural studies and thermal properties

The thermal behavior of poly(1-octene)s obtained at different monomer concentration, keeping constant the other polymerization conditions, was characterized by DSC. Fig. 1a shows the cooling behavior of poly(1-octene)s starting from homogeneous melt conditions. The crystallization behavior of all the polymers exhibits characteristic bimodal exotherms that are similar to those displayed by ethylene/α-olefin copolymers with a wide distribution of short chain branching [45,46]. The cooling DSC trace shows a relative sharp crystallization exotherm followed by a wide tail. The first peak corresponds to the crystallization of the linear portions of the less branched macromolecular chains that usually crystallize at higher temperatures, while the low temperature tail corresponds to the crystallization of the shorter linear portions of chains. The crystallization temperature (T_c) taken at the maximum of the sharp peak decreases with the increase of the monomer concentration (Table 2).

The heating curves of the non-isothermal crystallized poly(1-octene)s are reported in Fig. 1b. Glass transition events at low temperature and very broad melting endotherms can be observed. The glass transition temperature (T_g) ranges from -55 to -42 °C and decreases with increasing the monomer concentration (Table 2). The melting event begins at subambient temperatures and may extend over a 80°C temperature range. The broad endothermic event reflects the crystallization behavior pointing out the non-homogeneous distribution of the crystallizable units along the polymer chains. In general, as the monomer concentration increases the melting event of the obtained polymer shift to a lower temperature range and the melting point taken at peak maximum decreases (T_m in Table 2). Analogously, the melting enthalpy (ΔH_m) decreases with monomer concentration, going from 36 J/g for [1-octene] = 0.2 mol/L to 14 J/g for [1-octene] = 3 mol/L, reflecting the reduced crystallinity.

The influence of Al/Ni ratio on the thermal properties of poly(1-octene)s is analogous with previous observations deduced from monomer concentration effect. Indeed, an increase in the Al/Ni ratio from 10 to 200 produced a corresponding decrease in T_g, T_c, T_m, and ΔH_m of the polymer (Supporting Information Fig. S1). A further increase in Al/Ni ratio did not result in modifying the thermal properties of the polymer (Table 2 entry 12).

The thermal properties of the poly(1-octene)s obtained by varying the polymerization temperature are markedly different (Supporting Information Fig. S2). The polymer prepared at 0 °C exhibits a broad T_m at 44 °C with a cristallinity of 6.6%, while the polymer obtained at 50 °C

exhibits a T_m at 49°C with a cristallinity of 9.7%. In general, the reduction of the polymerization temperature results in a decrease in T_g, T_c, T_m, and ΔH_m of the polymer (Table 2 entry 5, 13, 14). Polymerizations carried out in the presence of MAO or MMAO at [1-octene] = 1 mol/L lead to polymers with a very low crystallinity. (Table 2 entry 15, 16). The melting range of these poly(1-octene)s was very broad and located at a much lower temperature, beginning at about -25 °C and ending near 60 °C, as compared to the polymers prepared by Ni-1/Et_2AlCl (Supporting Information Fig. S3).

Concerning the polymers microstructure, the total branching was first calculated by ^1H NMR. The exclusive 1,2-enchainment would result in a poly(1-octene) with 125 branches/1000C but the observed trend is that the branching content was almost half of the theoretic value, which is a result of nickel migration on polymer chain [47]. All the polymers were also characterized by ^{13}C NMR for quantification of total methyl groups, and branch-type distribution [40]. The results are summarized in Table 2. Typical spectrum of a branched polymer obtained with Ni-1/Et_2AlCl (Table 1 entry 1) is shown in Fig. 2. Interpretation of the ^{13}C NMR spectra was performed on the basis of previously assignments [36]. The nomenclature used for isolated branches is that of Usami and Takayama [48]. All the investigated polymers have predominantly methyl and longer than butyl branches (Me and Lg in Table 2, respectively): the intense signal at 27.73 ppm of long methylene –CH_2– sequences and signals due to methyl ($1B_1$ at 17.86 ppm) and longer branches ($1B_n$ at 12.01 ppm and $2B_n$ at 20.68 ppm) are safely identified in the ^{13}C NMR spectra. Carbons of ethyl and butyl branch ($1B_2$ and $2B_4$ at 9.0 and 21.1 ppm, respectively) are absent, while a very weak signals due to a propyl branch ($1B_3$ at 12.86 ppm) is observed and ascribed to a small fraction of 1,2-monomer insertion into a secondary Ni-alkyl bond [44]. Propyl branches are present in less than 3.0 mol%. In addition, after a careful analysis of the ^{13}C NMR spectra, the occurrence of methyl signals were registered in the region spanning from 14 to 15 ppm (marked as T in Fig. 2). Sivaram assigned all of these peaks to carbons of adjacent methyl branches [49], while Brookhart observed how some of these signals could also be ascribed to methyl groups adjacent to longer branches [39].

The overall trend was that the 8,1-enchainment, which gave to linear polymer chain segments (Scheme 1), ranged from 48 to 62% without any apparent relation with respect to the polymerization conditions and the aluminum alkyl employed. This suggest that the catalyst system did not have a significant selectivity for 2,1- and 1,2-insertion.

With respect to the results obtained by varying the concentration of 1-octene, the overall trend is that increasing the monomer concentration results in relatively constant total methyls. In contrast, monomer concentration significantly determines the branch-type distribution. The formation of a longer than methyl branch was favoured by increasing the 1-octene loading, while

methyl branches dominated at low monomer concentration. The predominance of methyl branches means that 1,2-insertion followed by chain-walking (ω,2-enchainment) is much faster than successive 1,2-insertions (1,2-enchainment) (Scheme 1) [36,40,50].

Comparison of the polymers obtained at different polymerization temperature shows that the content of methyl-type branches increases from 14 to 39 CH_3/1000C when the temperature was increased, while longer branches decreased from 50 to 22 CH_3/1000C. This indicates that an increase in reaction temperature accelerates ω,2-enchainment with respect to 1,2-enchainment, while the 8,1-enchainment percentage ranges from 53 to 57, confirming that Ni-1/Et_2AlCl catalyst system did not have a selectivity for 1,2- and 2,1-insertion.

When MAO or MMAO alumoxane was used, the 8,1-enchainment (2,1-insertion followed by chain-walking) content was almost the same found for Et_2AlCl. This means that the selectivity for 1,2- and 2,1-insertion was relatively independent from the aluminum alkyl employed. However, the resulting polymers had a different branch-type distribution. In particular, Ni-1/MAO and Ni-1/MMAO catalysts gave polymers with a larger fraction of long branches (Table 2), while Ni-1/Et_2AlCl gave polymers with a larger fraction of methyl ones. This means that Ni-1/MAO and Ni-1/MMAO catalysts show a higher selectivity for 1,2-insertion followed by a new monomer insertion (1,2-enchainment), while Ni-1/Et_2AlCl shows a higher selectivity for 1,2-insertion followed by chain-walking to give a methyl branch (ω,2-enchainment). Such differences may be also due to the nature of the ion pairing species generated from the two aluminum alkyls. Indeed, the anion generated from the reaction of Ni-1 with Et_2AlCl is smaller than that from MAO or MMAO, validating a closer interaction with the active center, and forcing the 1,2-interted unit to chain-walk before a new 1,2-insertion [42].

As well known, the thermal properties and crystallinity of polymers are strongly influenced by microstructure. Indeed, the poly(1-octene)s exhibit noticeable differences in melting temperature and crystallinity even comparing polymers with the same content of total branching. Fig. 3a plots T_m versus the sum of all the branches longer than methyl for the polymers under investigation. A relationship between the two data was found and increasing the content of longer side groups the melting temperature decreases. An analogous trend was observed for melting enthalpy. It is worth noting that, with the same branches longer than methyl content, the polymers produced by Ni-1/MAO and Ni-1/MMAO exhibit lower T_m and crystallinity than those obtained by Ni-1/Et_2AlCl. These features could be attributed to a different distribution of the long chain branches along the polymer chains.

The synthesized poly(1-octene)s were structurally characterized by X-ray techniques. WAXD patterns show a diffuse peak centered at about 20 2θ°, while the typical diffractions of the

orthorhombic poly(ethylene) crystalline phase are not evidenced (Supporting Information Fig. S4). Therefore, the low melting temperature and broad melting range of poly(1-octene)s are attributed to the fringed-micellar crystal structure with a broad size distribution that come from the statistical distribution of crystallizable chain lengths [51,52].

SAXS data were elaborated to calculate the internal surface (O_s) considering that the crystallinity of the polymers was due to the presence of fringed micellar crystals, consisted of bundles of parallel chain segments randomly dispersed in an amorphous matrix. The internal surface generally decreases as a function of the polymer crystallinity. Nevertheless, the O_s values calculated for the polymers produced by Ni-1/MAO and Ni-1/MMAO resulted significantly lower than those prepared by Ni-1/Et_2AlCl with similar branches longer than methyl content (Fig. 3b). These results resemble the trends observed for T_m vs. long branching relationships, suggesting a different morphology of the polymers in terms of dimension of fringed-micellar crystals and their dispersion in the amorphous matrix.

Another important parameter, strictly related to the polymer topology, is the intrinsic viscosity ($[\eta]_w$ in Table 1). The $[\eta]_w$ generally increases as a function of the polymer molecular weight. Nonetheless, the $[\eta]_w$ values for the polymers obtained from Ni-1/MAO and Ni-1/MMAO resulted lower than those from Ni-1/Et_2AlCl with comparable molecular weight, indicating a different polymer topology [53].

3.3 Uniaxial tensile properties

Preliminary investigation on mechanical behavior of poly(1-octene)s was carried at 20 °C out by uniaxial stretching until failure. The polymers exhibit elastomeric features with a low modulus, a uniform deformation to high strain and an instantaneous strain recovery after fracture. The tensile properties are reported in Table 3 and selected stress-strain curves are shown in Fig. 4.

Comparing the tensile behaviours of polymers obtained by Ni-1/Et_2AlCl varying the polymerization parameters, *i.e.*, monomer feedstock concentration, reaction temperature and Al/Ni ratio, one can notice some remarkable differences. The initial modulus depends only on the crystallinity of the polymer ranging from 9 to 2 MPa with decreasing the crystallinity. Most of the polymers show high and comparable ultimate strain (about 1250±150%), independent of the crystallinity. A stress upswing, characterized by an increasing slope in the stress-strain curve, was observed for most of the materials with ultimate tensile strength in the range from 8 to 14 MPa. Samples 1 and 13 show a different tensile behavior with very low elongation at break and ultimate tensile strength. Conversely, the poly(1-octene)s obtained by Ni-1/MAO and Ni-1/MMAO exhibited a nearly constant stress, *i.e.* no stress upswing, yet a large strain, 1200 and 800% for entry

15 and 16, respectively (Fig. 4). The elastic modulus of both polymers is low in agreement with their very low crystallinity (Table 3).

The elasticity of the poly(1-octene)s, *i.e.* the capability to return to the initial state once the force is removed, was evaluated from step cycle tensile tests. In the first set of experiments, the samples were cyclically loaded and unloaded ten times to 300% strain. All the poly(1-octene)s exhibit a certain amount of unrecovered strain after the 1st cycle with only a small increase in the unrecovered strain on each subsequent cycle. For example, the cyclic curve of sample 8 is shown in Fig. 5. For all the polymers, a permanent structural change took place during the 1st cycle, and a material with better elastomeric properties was created. The main difference between the cyclic deformation behavior of the poly(1-octene)s is in the amount of unrecovered strain after the 1st cycle. From the stress-strain curve the strain recovery (SR) can be calculated as $SR = 100\ (\varepsilon_a - \varepsilon_r)/\ \varepsilon_a$, where ε_a is the applied strain and ε_r is the strain in the cycle at zero load after the applied strain. The recovery strain after the first load cycle ranges from 50 to 86% and increases with decreasing the polymer crystallinity (SR_1 in Table 3). All the polymers show a slight decreasing trend in the strain recovery with the load cycle times, whereas the order of the strain recovery remains unchanged (Fig. 6). The more amorphous poly(1-octene)s displayed excellent elastic recoveries of about 75% after the last load cycle (SR_X in Table 3). It is worth pointing out that for the hysteresis test performed at fixed 300% strain, the polymers produced by Ni-1/MAO and Ni-1/MMAO behave in-line with those obtained by Ni-1/Et_2AlCl, exhibiting a similar strain recovery trend.

In the second set of cyclic experiments, the samples were extended step by step up to different strains. As a typical example, the stress-strain curve during cyclic tensile deformation of sample 8 is shown in Fig. 7. The strain recovery is plotted as a function of the applied strain in Fig. 8. For all the materials obtained by Ni-1/Et_2AlCl, the strain recovery decreases rapidly at lower applied strains and then levels off at higher applied strains. Generally, the elastic recovery over the whole range of deformations decreases with increasing the crystallinity of the polymer. Entry 9, *i.e.* the more amorphous polymer produced by Ni-1/Et_2AlCl at [1-octene] = 3 mol/L, exhibits the highest elastic recovery (about 78%) for the whole range of applied strains. The dependence of strain recovery on the applied deformation was somewhat different for the polymers obtained by Ni-1/MAO and Ni-1/MMAO. For entry 15 and 16, the strain recovery decreased linearly with increasing the applied strain over the entire cyclic test (Supporting Information Fig. S5).

Overall, the tensile tests showed that the investigated polymers behave as thermoplastic elastomers with properties close to those reported for block and random poly(ethylene-*co*-1-octene) [8, 54-56], and generally outperform the 1-dodecene/ethylene di- and tri-block copolymers in

terms of elastic recovery [36]. Moreover, it is worth emphasizing that these materials retain excellent mechanical properties even after being molted and reprocessed several times (Supporting Information Fig. S6).

4. Conclusions

The α-diimine Ni-1 complex, in combination with an aluminum alkyl, polymerize 1-octene in high yield to semicrystalline, branched poly(ethylene)–like materials with high molecular weight and narrow molecular weight distribution. The polymers are mainly composed of methyl branches formed by 1,2-monomer insertion followed by chain-walking (ω,2-enchainment), and longer than hexyl branches formed by successive 1,2-insertions (1,2-enchainment). The extent of chain-walking can be easily tuned by varying the polymerization conditions and reagents. The monomer concentration and the polymerization temperature dictate the competition between the two mechanisms: the 1,2-enchainment is much faster than the ω,2-enchainment at high 1-octene concentration, while an increase in reaction temperature accelerates ω,2-enchainment with respect to successive 1,2-insertions. By varying the aluminum alkyl, the content of 8,1-enchainment to give the linear polymer segment does not vary, indicating that there is no selectivity towards a 1,2- or 2,1-insertion. However, the Ni-1 complex, in combination with MAO or MMAO, gives polymers with a larger fraction of long branches, while, when activated with Et_2AlCl, exhibits a higher selectivity for 1,2-insertion followed by chain-walking to give a methyl branch.

The thermal properties and crystallinity of the poly(1-octene)s are strongly determined by their microstructure. A relationship between the melting behavior and the content of branches longer than methyl was found: increasing the content of long side groups the melting temperature decreases. The polymers produced by Ni-1/MAO and Ni-1/MMAO exhibit lower crystallinity and melting temperature than those from Ni-1/Et_2AlCl, owing to a different distribution of the long chain branches along the polymer chains.

The tensile tests showed that the poly(1-octene)s behave as TPEs exhibiting a low modulus, a uniform deformation to high strain and an instantaneous strain recovery after fracture. The Young's modulus of the polymers obtained by Ni-1/Et_2AlCl increases with the crystallinity, while the ultimate strain and tensile strength result quite constant. The poly(1-octene)s obtained by Ni-1/MAO and Ni-1/MMAO exhibit a large strain and a nearly constant low stress. The hysteresis tests showed that the elastic recovery of the poly(1-octene)s is mainly influenced by their crystallinity. The high amourphous materials show excellent recovery for strain higher than 1200%.

Acknowledgements

The authors thank Adriana Cacciamani, Fulvia Greco and Daniele Piovani for skilled technical assistance and helpful discussion. This work was partly supported by the Ministero dell'Istruzione, dell'Università e della Ricerca (Italy), Progetto PON01_00074 DIATEME.

Appendix A. Supplementary material

Supplementary data associated with this article can be found, in the online version, at …

References

[1] W. Kaminsky, Polyolefins: 50 years after Ziegler and Natta I: Polyethylene and polypropylene; W. Kaminsky, Ed.; Springer, New York, 2013.
[2] J. Klosin, P.P. Fontaine, R. Figueroa, Acc. Chem. Res. 48 (2015) 2004-2016.
[3] M.C. Baier, M.A. Zuideveld, S. Mecking, Angew. Chem. Int. Ed. 53 (2014) 9722-9744.
[4] J. P. McInnis, M. Delferro, T. J. Marks, Acc. Chem. Res. 47 (2014) 47 2545-2557.
[5] G.W. Coates, P.D. Hustad, S. Reinartz, Angew. Chem., Int. Ed. 41 (2002) 2236-2257.
[6] M. Stürzel, S. Mihan, R Mülhaupt, Chem. Rev. 116 (2016) 1398-1433.
[7] Y. Chen, L. Wang, H. Yu, Y. Zhao, R. Sun, G. Jing, J. Huang, H. Khalid, N. M. Abbasi, M. Akram, Prog. Polym. Sci. 45 (2015) 23-43.
[8] H.P. Wang, S.P. Chum, A. Hiltner, E. Baer, J. Appl. Polym. Sci. 113 (2009) 3236-3244.
[9] J. Minick, A. Moet, A. Hiltner, E. Baer, S.P. Chum, J. Appl. Polym. Sci. 58 (1995) 1371-1384.
[10] H.P. Wang, D.U. Khariwala, W. Cheung, S.P. Chum, A. Hiltner, E. Baer, Macromolecules 40 (2007) 2852-2862.
[11] G.W. Coates, R.M. Waymouth, Science 267 (1995) 217-219.
[12] D.J. Arriola, E.M. Carnahan, P.D. Hustad, R.L. Kuhlman, T.T. Wenzel, Science 312 (2006) 714-719.
[13] A.H. Dekmezian, J.B.P. Soares, P.J. Jiang, C.A. Garcia-Franco, W.Q. Weng, H. Fruitwala, T. Sun, D.M. Sarzotti, Macromolecules 35 (2002) 9586-9594.
[14] W.Q. Weng, E.J. Markel, A.H. Dekmezian, Macromol. Rapid Commun. 21 (2000) 1103-1107.

[15] H. Ohtaki, F. Deplace, G.D. Vo, A.M. LaPointe, F. Shimizu, T. Sugano, E.J. Kramer, G.H. Fredrickson, G.W. Coates Macromolecules 48 (2015) 7489-7494.
[16] A. Hotta, E. Cochran, J. Ruokolainen, V. Khanna, G.H. Fredrickson, E.J. Kramer, Y.W. Shin, F. Shimizu, A.E. Cherian, P.D. Hustad, J.M. Rose, G.W. Coates, Proc. Natl. Acad. Sci. U.S.A. 103 (2006) 15327-15332.
[17] K.E. Crawford, L.R. Sita, ACS Macro Lett. 4 (2015) 921-925.
[18] S. Wang, W.H. Sun, C.J. Redshaw, Organomet. Chem. 751 (2014) 717-741.
[19] D.H. Camacho, Z. Guan, Chem. Commun. 46 (2010) 7879-7893.
[20] G.J. Domski, J.M. Rose, G.W. Coates, A.D. Bolig, M. Brookhart, Prog. Polym. Sci. 32 (2007) 30-92.
[21] Z. Ye, L. Xu, Z. Dong, P. Xiang, Chem. Commun. 49 (2013) 6235-6255.
[22] Z. Dong, Z. Ye, Polym. Chem. 3 (2012) 286-301.
[23] Z. Ye, W. Feng, S. Zhu, Dong, Q. Yu, Macromol. Rapid Commun. 27 (2006) 871-876.
[24] P. Xiang, Z. Ye, S. Morgan, X. Xia, W. Liu, Macromolecules 42 (2009) 4946-4949.
[25] L.K. Johnson, C.M. Killian, M. Brookhart, J. Am. Chem. Soc. 117 (1995) 6414-6415.
[26] G. Leone, S. Losio, D. Piovani, A. Sommazzi, G. Ricci, Polym. Chem. 3 (2012) 1987-1990.
[27] D.P. Gates, S.A. Svejda, E. Onate, C.M. Killian, L.K. Johnson, P.S. White, M. Brookhart, Macromolecules 33 (2000) 2320-2334.
[28] F. Wang, R. Tanaka, Z. Cai, Y. Nakayama, T. Shiono, Polymers 8 (2016) 160.
[29] C. Wen, S. Yuan, Q. Shi, E. Yue, D. Liu,W.H. Sun, Organometallics 33 (2014) 7223-7231.
[30] H. Hu, H. Gao, D. Chen, G. Li, Y. Tan, G. Liang, F. Zhu, Q. Wu, ACS Catal. 5 (2015) 122-128.
[31] J.L. Rhinehart, L.A. Brown, B.K. Long, J. Am. Chem. Soc 135 (2013) 16316-16319.
[32] S. Dai, X. Sui, C. Chen, Angew. Chem. Int. Ed. 54 (2015) 1-7.
[33] S. Takano, D. Takeuchi, K. Osakada, Chem. Eur. J. 21 (2015) 16209-16218.
[34] K.E. Allen, J. Campos, O. Daugulis, M. Brookhart, ACS Catal. 5 (2015) 456-464.
[35] J.M. Rose, F. Deplace, N.A. Lynd, Z. Wang, A. Hotta, E.B. Lobkovsky, E.J. Kramer, G.W. Coates, Macromolecules 41 (2008) 9548-9555.
[36] G. Leone, M. Mauri, F. Bertini, M. Canetti, D. Piovani, G. Ricci, Macromolecules 48 (2015) 1304-1312.
[37] L.K. Johnson, C.M. Killian, M. Brookhart, J. Am. Chem. Soc. 117 (1995) 6414-6415.
[38] D. Meinhard, M. Wegner, G. Kipiani, A. Hearley, P. Reuter, S. Fischer, O. Marti, B. Rieger, J. Am. Chem. Soc. 129 (2007) 9182-9191.

[39] E.F. McCord, S.J. McLain, L.T.J. Nelson, S.D. Ittel, D. Tempel, C.M. Killian, L.K. Johnson, M. Brookhart, Macromolecules 40 (2007) 410-420.
[40] J.D. Azoulay, G.C. Bazan, G.B. Galland, Macromolecules 43 (2010) 2794-2800.
[41] O. Glatter, O. Kratky, Small Angle X-ray Scattering. Academic Press, London, 1982.
[42] H.Y. Gao, X.F. Liu, Y. Tang, J. Pan, Q. Wu, Polym. Chem. 2 (2011) 1398-1403.
[43] R.F. de Souza, L.C. Simon, M.D.C.M. Alves, J. Catal. 214 (2003) 165-168.
[44] J. Merna, Z. Hoštálek, J. Peleška, J. Roda, Polymer 50 (2009) 5016-5023.
[45] M. Canetti, G. Leone, G. Ricci, F. Bertini Eur. Polymer J. 73 (2015) 423-432.
[46] W. Liu, W.J. Wang H. Fan, L. Yu, B.G. Li, S. Zhu, Eur. Polym. J. 54 (2014) 160-171.
[47] S.D. Ittel, L.K. Johnson, M. Brookhart, Chem. Rev. 100 (2000) 1169-1203.
[48] T. Usami, S. Takayama, Macromolecules 17 (1984) 1756-1761.
[49] U. Subramanyam, P.R. Rajamohanan, S. Sivaram, Polymer 45 (2004) 4063-4076.
[50] T. Vaidya K. Klimovica, A.M. LaPointe, I. Keresztes, E.B. Lobkovsky, O. Daugulis, G.W. Coates, J. Am. Chem. Soc. 136 (2014) 7213-7216.
[51] H.P. Wang, S.P. Chum, A. Hiltner, E. Baer, J. Polym. Sci. Part B: Polym. Phys. 47 (2009) 1313-1330.
[52] A. Alizadeh, L. Richardson, J . Xu, S. McCartney, H. Marand, Y.W. Cheung, S. Chum, Macromolecules 32 (1999) 6221-6235.
[53] P.M. Cotts, Z. Guan, E. McCord, S. McLain, Macromolecules 33 (2000) 6945-6952.
[54] W. Liu, X. Zhang, Z. Bu W.J. Wang H. Fan, B.G. Li, S. Zhu, Polymer 72 (2015) 118-124.
[55] S. Hölzer, M. Menzel, Q. Zia, U.S. Schubert, M. Beiner, R. Weidisch, Polymer 54 (2013) 5207-5213.
[56] F. Zuo, C. Burger, X. Chen, Y. Mao, B. Hsiao, H. Chen, G.R. Marchand, S.Y. Lai, D. Chiu, Macromolecules 43 (2010) 1922-1929.

Table 1. Polymerization of 1-octene catalyzed by Ni-1[a].

entry	OCT (mol/L)	Al-alkyl	Al/Ni (mol/mol)	T (°C)	Yield (g)	Conv (%)	TOF[b] (h^{-1})	M_n[c] (kg/mol)	M_w/M_n[c]	$[\eta]_w$[d] (dL/g)
1[e]	0.2	Et_2AlCl	200	22	0.19	54	59	36.6	1.16	0.34
2[e]	0.4	Et_2AlCl	200	22	0.40	56	118	74.0	1.20	0.62
3	0.6	Et_2AlCl	200	22	0.59	55	175	90.8	1.29	0.69
4	0.8	Et_2AlCl	200	22	0.82	58	244	101.8	1.32	0.65
5[e]	1.0	Et_2AlCl	200	22	1.10	58	327	105.6	1.36	0.94
6[e]	1.5	Et_2AlCl	200	22	1.73	65	514	109.1	1.68	0.95
7	2.0	Et_2AlCl	200	22	2.43	68	722	132.6	1.64	1.34
8[e]	2.5	Et_2AlCl	200	22	2.99	67	888	175.0	1.73	1.36
9	3.0	Et_2AlCl	200	22	3.16	59	862	230.0	1.84	1.60
10	1.0	Et_2AlCl	10	22	1.20	67	328	100.4	1.37	0.86
11	1.0	Et_2AlCl	50	22	1.24	69	338	114.7	1.40	0.93
12	1.0	Et_2AlCl	500	22	1.31	73	358	87.6	1.89	0.92
13	1.0	Et_2AlCl	200	0	0.33	18	90	80.5	1.23	0.67
14	1.0	Et_2AlCl	200	50	1.24	69	338	132.1	1.78	0.90
15	1.0	MMAO	200	22	0.74	42	202	142.7	1.65	0.81
16	1.0	MAO	200	22	0.72	40	197	167.5	1.51	1.07

[a] Polymerization conditions: toluene, total volume, 18 mL; Ni-1, 10 μmol; time, 180 min.

[b] Turnover frequency (TOF), calculated by the equation: $mol_{pol} \times mol_{Ni}^{-1} \times h^{-1}$.

[c] Molecular weight (M_n) and molecular weight distribution (M_w/M_n) from SEC.

[d] Weight-average intrinsic viscosity ($[\eta]_w$) by SEC using the online viscometer.

[e] Data reported in [36].

Table 2. Microstructural data and thermal properties. CH_3/1000C [c]

entry	branches/ 1000C[a]	8,1[b] (%)	CH_3/1000C [c]		total CH_3[c]	T_g[d] (°C)	T_c[d] (°C)	T_m[d] (°C)	ΔH_m[d] (J/g)	X_{DSC}[e] (%)
			Me	Lg						
1	74	48	35	22	59	-42	43	57	36	12.4
2	68	52	34	26	61	-45	34	55	29	10.0
3	59	58	32	27	60	-45	33	54	26	9.9
4	61	57	33	29	63	-46	33	53	25	8.6
5	66	53	27	32	60	-49	31	49	22	7.6
6	64	55	22	37	60	-51	27	45	19	6.6
7	62	56	20	42	63	-50	26	44	18	6.2
8	65	54	18	41	60	-50	25	43	18	6.2
9	71	50	16	49	66	-55	22	39	14	4.8
10	58	58	32	26	60	-44	38	56	33	11.4
11	53	62	29	28	58	-46	36	54	31	10.7
12	67	53	32	31	63	-49	30	48	22	7.6
13	60	57	14	50	64	-56	23	44	19	6.6
14	61	57	38	24	62	-44	34	51	28	9.7
15	67	53	24	43	68	-53	18	36	10	3.4
16	69	51	21	48	70	-55	14	31	8	2.8

[a] From ^{1}H NMR (Supporting Information eq.1).

[b] Percentage of 8,1-insertion (Supporting Information eq.2).

[c] From ^{13}C NMR. A small amount (never exceeding 2 CH_3/1000C) of propyl branches was observed.

[d] From DSC.

[e] Crystallinity from melting enthalpy, $X_{DSC} = (\Delta H_m/\Delta H^0_m)\times 100$, $\Delta H^0_m = 290$ J/g.

Table 3. Mechanical properties.

Entry	E[a] (MPa)	σ[a] (MPa)	ε[a] (%)	SR_I[b]	SR_X[c]	$SR_{1200\%}$[d]
1	9.3±0.2	1.4±0.1	30±4	-	-	-
2	6.8±0.8	2.3±0.2	560±35	50	35	n.d.[e]
3	6.5±0.3	4.1±0.3	1179±62	60	46	45
4	5.7±0.4	5.1±0.3	1148±30	61	48	50
5	5.1±0.3	8.6±0.8	1350±12	66	54	59
6	4.7±0.1	9.1±0.7	1282±91	74	64	69
7	3.8±0.3	8.6±0.7	1198±55	81	71	73
8	3.7±0.3	9.4±0.3	1284±32	82	74	74
9	3.3±0.1	8.0±0.4	1300±66	86	78	78
10	7.8±1.3	13.8±1.8	1337±88	56	43	48
11	5.9±0.1	11.8±0.5	1173±26	57	45	52
12	4.9±0.2	8.6±1.5	1388±89	66	54	61
13	2.3±0.3	0.9±0.1	146±21	-	-	-
14	5.7±0.3	9.4±0.9	1200±54	57	43	53
15	3.5±0.7	1.9±0.3	1210±60	81	69	n.d.[e]
16	2.3±0.2	1.7±0.4	800±42	85	75	n.d.[e]

[a] E = Young's modulus, σ = ultimate tensile strength, ε = elongation at break.

[b] Strain recovery measured after the first step in a step cycle test type at 300% strain.

[c] Strain recovery measured after the last step in a step cycle test type at 300% strain.

[d] Strain recovery measured after the strain at 1200% in a step cycle test type at increasing strains.

[e] The specimens break before the strain at 1200% in a step cycle test type at increasing strains.

Figure Captions

Scheme 1.

Possible polymerization mechanisms for 1-octene polymerization by Ni(II) complexes.

Fig. 1.

DSC cooling scans (a) and DSC successive heating scans (b) of selected poly(1-octene)s obtained at different monomer feedstock concentration.

Fig. 2.

^{13}C NMR spectrum and assignment of a selected poly(1-octene) (Table 1, entry 1). The polymer was dissolved in $C_2D_2Cl_4$, and HDMS was used as internal chemical shift reference.

Fig. 3.

Plot of (a) melting temperature (T_m) and (b) internal surface (O_s) as a function of the total branching longer than methyl. The solid lines are guides to the eye and illustrate the overall trend.

Fig. 4.

Stress-strain curves of selected poly(1-octene)s during monotonic tensile deformation.

Fig. 5.

Stress-strain curve of poly(1-octene) (Table 1, entry 8) in the hysteresis experiments for a strain of 300%.

Fig.6.

Strain recovery as a function of cycle times of the poly(1-octene)s obtained at different monomer concentration (entries 2-9 from bottom to top).

Fig.7.

Stress-strain curve of poly(1-octene) (Table 1, entry 8) during step cycle tensile deformation at different strain.

Fig.8.

Strain recovery as a function of the applied strain of the poly(1-octene)s obtained at different monomer concentration (entries 2-9 from bottom to top).

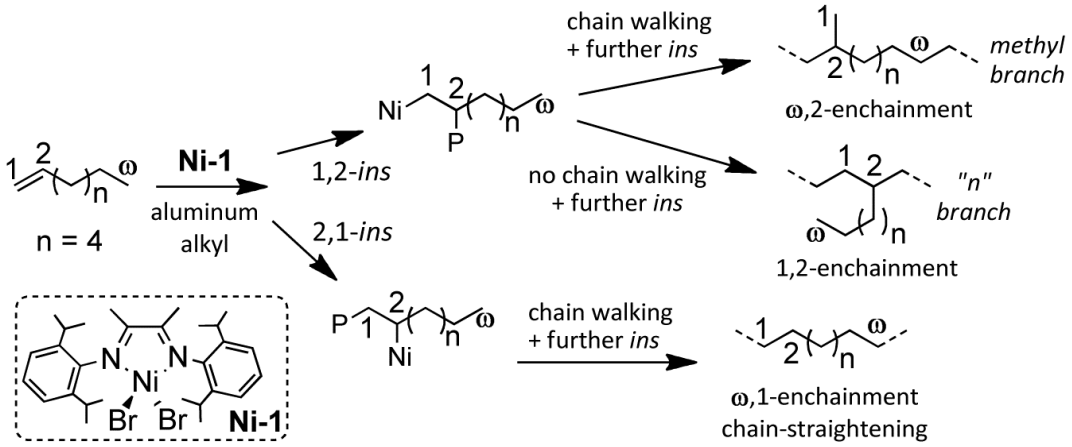

Scheme 1. Possible polymerization mechanisms for 1-octene polymerization by Ni(II) complexes.

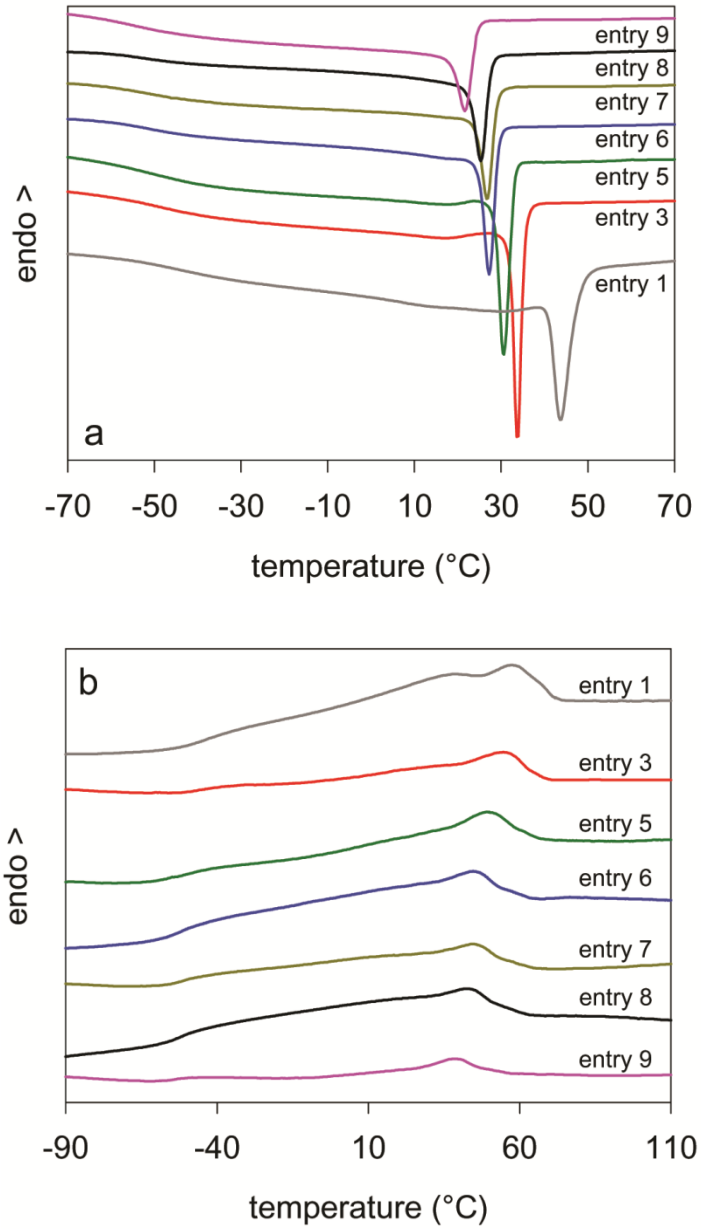

Figure 1. DSC cooling scans (a) and DSC successive heating scans (b) of selected poly(1-octene)s obtained at different monomer feedstock concentration.

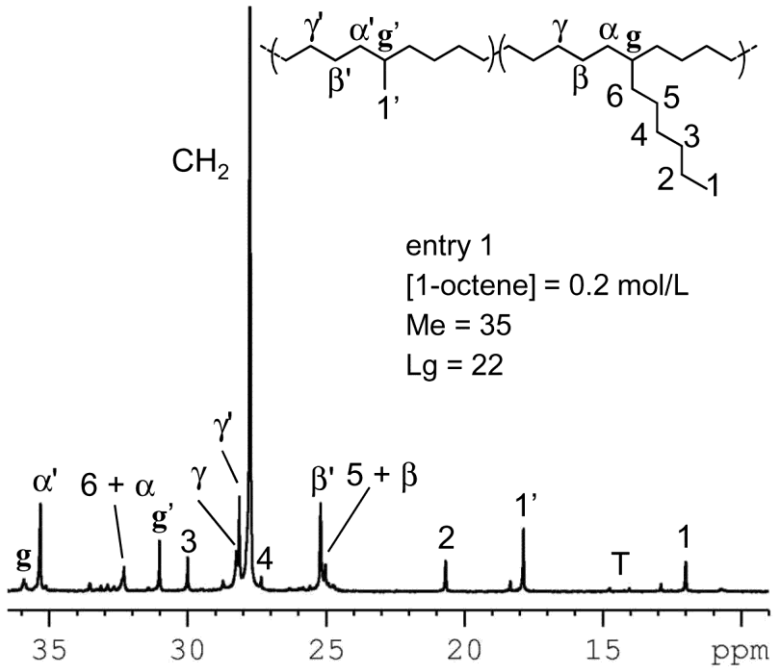

Figure 2. ^{13}C NMR spectrum and assignment of a selected poly(1-octene) (Table 1, entry 1). The polymer was dissolved in $C_2D_2Cl_4$, and HDMS was used as internal chemical shift reference.

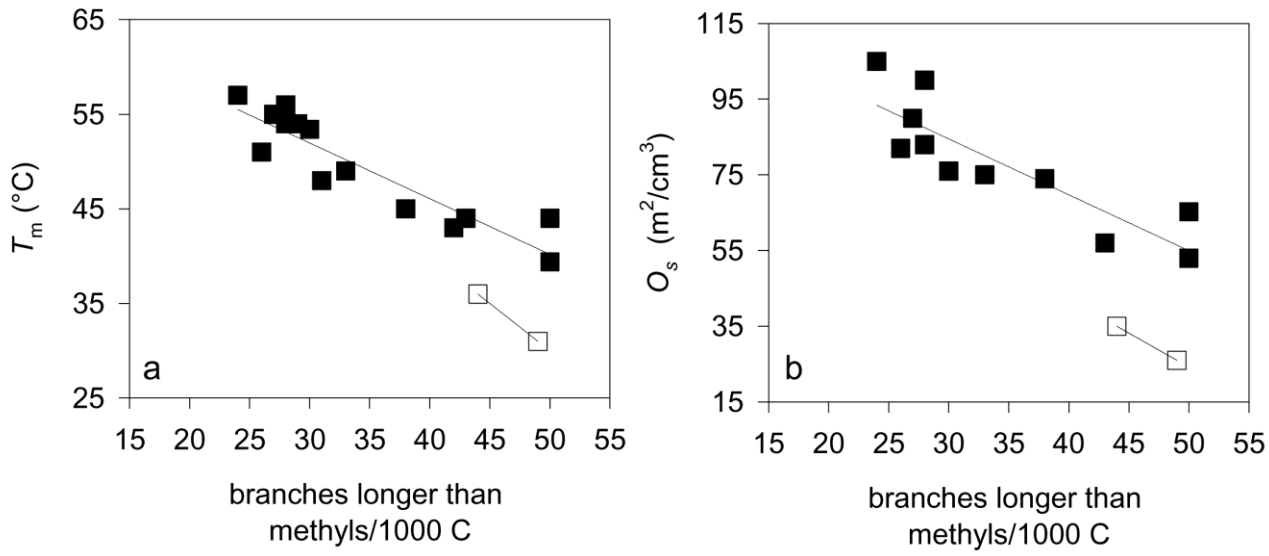

Figure 3. Plot of (a) melting temperature (T_m) and (b) internal surface (O_s) as a function of the total branching longer than methyl. The solid lines are guides to the eye and illustrate the overall trend.

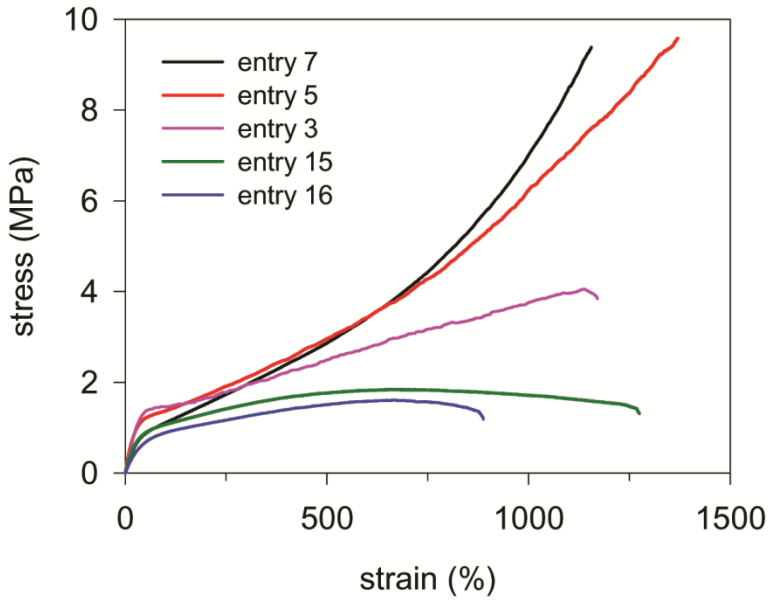

Figure 4. Stress-strain curves of selected poly(1-octene)s during monotonic tensile deformation.

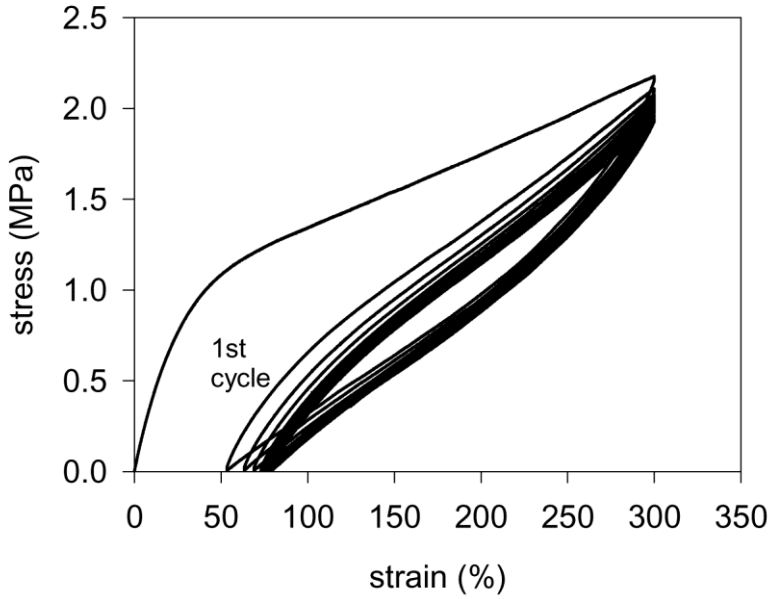

Figure 5. Stress-strain curve of poly(1-octene) (Table 1, entry 8) in the hysteresis experiments for a strain of 300%.

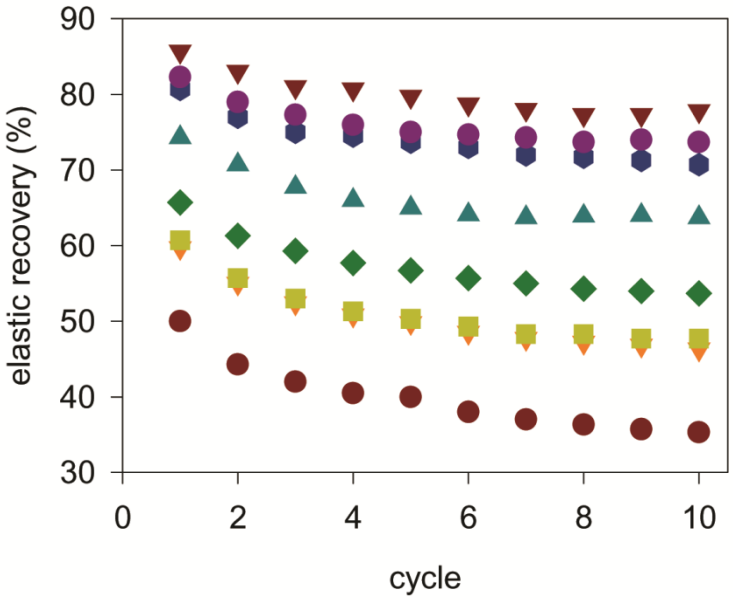

Figure 6. Strain recovery as a function of cycle times of the poly(1-octene)s obtained at different monomer concentration (entries 2-9 from bottom to top).

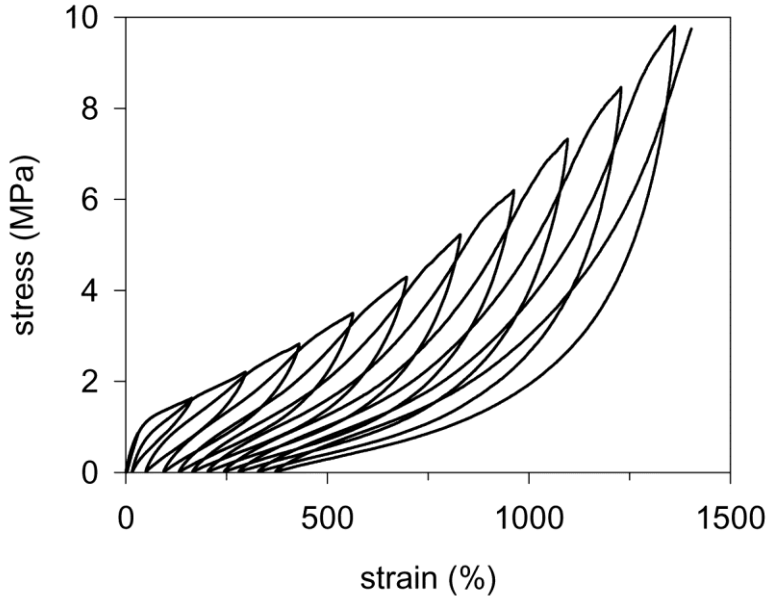

Figure 7. Stress-strain curve of poly(1-octene) (Table 1, entry 8) during step cycle tensile deformation at different strain.

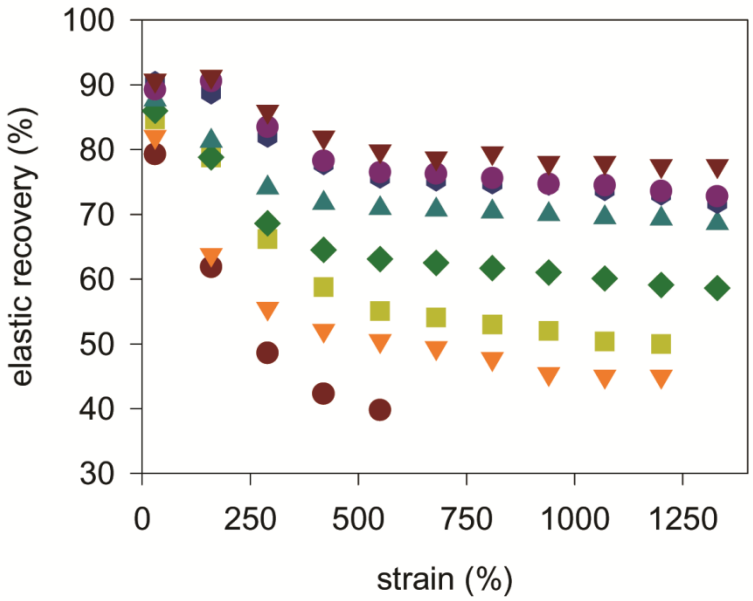

Figure 8. Strain recovery as a function of the applied strain of the poly(1-octene)s obtained at different monomer concentration (entries 2-9 from bottom to top).